Performance of DFT functionals for calculating the second-order nonlinear optical properties of dipolar merocyanines

Lescos, Laurie; Sitkiewicz, Sebastian P.; Beaujean, Pierre; Blanchard-Desce, Mireille; Champagne, Benoît; Matito, Eduard; Castet, Frédéric

Published in:
Physical Chemistry Chemical Physics

DOI:
10.1039/d0cp02992k

Publication date:
2020

Document Version
Publisher's PDF, also known as Version of record

PCCP

ROYAL SOCIETY OF CHEMISTRY

PAPER

View Article Online
View Journal | View Issue

Cite this: *Phys. Chem. Chem. Phys.*, 2020, **22**, 16579

Performance of DFT functionals for calculating the second-order nonlinear optical properties of dipolar merocyanines†

Laurie Lescos,[a] Sebastian P. Sitkiewicz,[bcd] Pierre Beaujean,[e] Mireille Blanchard-Desce,[a] Benoît Champagne,*[e] Eduard Matito*[bf] and Frédéric Castet*[a]

Received 3rd June 2020,
Accepted 7th July 2020

DOI: 10.1039/d0cp02992k

rsc.li/pccp

The second-order nonlinear optical responses of a series of recently designed dipolar merocyanines are investigated using the 2006 Minnesota family of hybrid exchange–correlation functionals (XCFs), as well as the LC-BLYP, ωB97XD and CAM-B3LYP long-range (LR) corrected XCFs. The performance of these different levels of approximation is discussed in regard to reference second-order Møller–Plesset calculations and experimental data obtained from Hyper-Rayleigh Scattering (HRS) measurements. Particular focus is given to the influence of the amount of exact Hartree–Fock exchange included in the XCF on the magnitude of the static HRS responses, as well as to the impact of tuning the range-separation parameter in LR-XCFs, according to a system-specific nonempirical procedure. Frequency dispersion effects are also investigated, as well as their crucial role in the comparison between theoretical and experimental data.

1 Introduction

The design of organic molecules that exhibit large quadratic nonlinear optical (NLO) responses has fueled a number of research works over the past thirty years, owing to their potential use as molecular components in optoelectronic devices or bioimaging. In particular, organic molecules exhibiting large first hyperpolarizability (β) are used as active elements in electric field poled polymer-based systems for electro-optic modulation,[1] or as probes for second-harmonic generation (SHG) imaging of lipid and cell membranes.[2–5] Although octupolar systems can also display large quadratic NLO responses,[6] high β values are most often associated to dipolar push–pull chromophores having a D–π–A architecture, in which an electron-donating group (D) interacts with an electron-withdrawing group (A) through a π-conjugated linker. These molecules usually display significant charge transfer between the D and A sites giving rise to intense absorption in the visible region. Varying the nature of the D and A groups or the length of the conjugated bridge by chemical design allows to modulate the magnitude of the second-order NLO responses.[7–11]

The first hyperpolarizability of molecular dyes is usually measured in dilute solutions using electric field-induced second harmonic generation (EFISHG) or Hyper-Rayleigh Scattering (HRS).[12] The total EFISHG response of π-conjugated systems is expressed as the sum of a second-order contribution $\beta_{\parallel}$ that corresponds to the projection of the vector part of β on the dipole moment vector, and of a third-order contribution $\gamma_{\parallel}$. Although the EFISHG second hyperpolarizability $\gamma_{\parallel}$ is usually neglected in experimental data analysis, recent calculations demonstrated that this contribution should not be omitted because it can be large, or even dominant, with respect to the second-order $\beta_{\parallel}$ counterpart.[13] On the other hand, HRS enables more direct estimates of the second-order NLO properties of push–pull compounds, without contamination of higher-order responses. As a complementary tool, computational chemistry provides rationales behind the magnitude of molecular NLO

[a] *Institut des Sciences Moléculaires (ISM, UMR CNRS 5255), University of Bordeaux, 351 Cours de la Libération, 33405 Talence, France. E-mail: frederic.castet@u-bordeaux.fr*
[b] *Donostia International Physics Center (DIPC), Manuel Lardizabal Ibilbidea 4, 20018 Donostia, Euskadi, Spain*
[c] *Kimika Fakultatea, Euskal Herriko Unibertsitatea (UPV/EHU), 20080 Donostia, Euskadi, Spain*
[d] *Institute of Computational Chemistry and Catalysis and Department of Chemistry, University of Girona, Campus de Montilivi, 17003 Girona, Catalonia, Spain*
[e] *Unité de Chimie Physique Théorique et Structurale, Chemistry Department, Namur Institute of Structured Matter, University of Namur, Belgium. E-mail: benoit.champagne@unamur.be*
[f] *Ikerbasque Foundation for Science, 48011 Bilbao, Euskadi, Spain. E-mail: ematito@gmail.com*

† Electronic supplementary information (ESI) available: Details on molecular geometries, optimal range separation parameters, absorption properties, static and dynamic second-order nonlinear optical properties. See DOI: 10.1039/d0cp02992k

responses, by giving insights on various factors not individually accessible from experiments. The latter include the impact of the nature of D and A groups, of the size of the π-conjugated linker, as well as of frequency-dispersion and solvent effects. For small polyatomic molecules, accurate descriptions of NLO properties are provided by coupled cluster (CC) calculations, the highest level of approximation employed so far for polyatomic molecules being CCSD(T), which includes single and double excitations together with a perturbative estimate of triples.[14,15] However, these methods cannot be routinely applied to large systems. Owing to its low computational cost, density functional theory (DFT) remains most often the only alternative for investigating the NLO properties of extended organic dyes of interest for real-life applications. Nevertheless, many works have reported the inadequacy of exchange–correlation functionals (XCFs) based on the local density approximation (LDA) or the generalized gradient approximation (GGA) for computing the first hyperpolarizabilities of extended systems. This failure has been attributed to the self-interaction error or overdelocalization of the response to external fields, and originates from the short-range treatment of exchange, as opposed to the exact exchange used in Hartree–Fock theory.[14,16,17] Global hybrid functionals incorporating a low amount of exact exchange were also proved unsuitable for the evaluation of β of conjugated chains terminated by D/A pairs, showing a nearly catastrophic behavior with respect to increasing the chain length.[16,18–20] This issue can be partially alleviated by using range-separated (RS) hybrids, which offer the possibility to restore the correct asymptotic behavior of the exchange potential at large distances.[14]

In this work, we explore the performance of various XCFs for predicting the quadratic NLO responses of recently designed dipolar merocyanines,[21–23] in which tricyanopropylidene-based acceptor units are connected to dihexylaminophenyl or dihexylaminothiophenyl donor moieties through polyenic bridges of different lengths (Fig. 1). HRS measurements demonstrated that these highly dipolar dyes exhibit large first hyperpolarizabilities together with an apparently antagonistic cyanine-like behavior. In particular, the longest derivative incorporating dihexylaminothiophenyl and phthalimide-substituted tricyanopropylidene terminal groups (**II′[4]**) was found to display a record hyperpolarizability together with a negligible bond length alternation (BLA),[21] in contradiction with the paradigm linking large quadratic NLO responses to an optimal, non zero BLA value.[8,9]

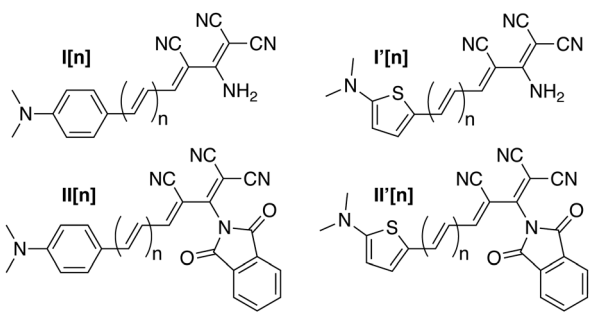

Fig. 1 Structures of the tricyanopropylidene-based merocyanines studied herein. The length of the polyenic chain varies from n = 0 to n = 4.

The accurate description of the first hyperpolarizabilities of such NLO chromophores, which exhibit large ground-state charge transfer as well as low-lying charge-transfer excited states, is highly challenging for DFT. Here, we examine the relevance of hybrid XCFs incorporating different rates of exact Hartree–Fock exchange (HFX), as well as of several RS hybrids. Since optimizing the range separation parameter ω in RS-XCFs has been shown to improve the description of first hyperpolarizabilities of some prototypical charge-transfer compounds,[19,20] hyperpolarizabilities calculated using default ω values are compared to those calculated using ω values tuned according to a system-specific, nonempirical procedure. Still, in this study, more complex, chemically-designed compounds are chosen in order to assess the performance of XCFs, extending the earlier works on prototypical systems like α,ω-nitro,amino-polyenes and -polyynes.[14,18] Here, the smallest compound (**I′[0]**) contains 30 atoms while the largest one (**II[4]**) has 61. The accuracy of the various functionals is discussed depending on their ability to reproduce experimental HRS data, as well as second-order Møller–Plesset (MP2) calculations, used as theoretical references.

2 Computational methods and reference experimental data

2.1 Levels of approximation

Molecular structures were optimized using density functional theory (DFT) together with the hybrid M06-2X[24] exchange–correlation (XCF) and the 6-311G(d) basis set. As shown in previous reports,[25,26] the M06-2X XCF reliably describes the bond length alternation (BLA) of extended π-conjugated systems, which is prerequisite for accurate predictions of optical properties. Each structure was characterized as a minimum on the potential energy surface based on its real harmonic vibrational frequencies. Note that terminal *N*,*N*-dihexylamino donor groups present in the compounds characterized experimentally have been replaced by simpler *N*,*N*-dimethylamino groups in all calculations (see Fig. 1).

Absorption properties, as well as static and dynamic (frequency-dependent) second-order nonlinear optical responses, were determined using time-dependent density functional theory (TDDFT)[27] with the 6-311+G(d) basis set in combination with various XCFs. The 2006 Minnesota family of functionals[24] was first considered, in order to evaluate the impact of increasing the amount of exact Hartree–Fock exchange (HFX) from M06L (0%) to M06 (27%), M06-2X (54%), and M06-HF (100%). The BLYP XCF was employed as well for comparison purposes. Since they have been shown to improve the description of second-order NLO properties of extended π-conjugated systems,[14,17,20] we also addressed the performance of different classes of long-range corrected (LRC) XCFs. Contrary to global hybrids in which the amount of exact HF exchange is fixed, LRC-XCFs, also referred to as range-separated (RS) hybrids, include HF exchange by means of a weighting function that depends on the interelectronic distance

r. The Coulomb operator is thus split into local and nonlocal parts using a smooth function (being the error function in the selection of XCFs considered herein) together with a range separation parameter ω, which damps the exchange contribution from the density functional and complements it with HF exchange:

$$\frac{1}{r} = \frac{1 - \alpha_1 - \alpha_2 \mathrm{erf}(\omega r)}{r} + \frac{\alpha_1 + \alpha_2 \mathrm{erf}(\omega r)}{r} \quad (1)$$

Thus, at long range, the amount of HFX equals $\alpha_1 + \alpha_2$, and subsequently the amount of DFT exchange equals $1 - \alpha_1 - \alpha_2$. The parameter α_1 allows, if non zero, to retain a fraction of DFT exchange in the asymptotic limit. The LRC-XCFs considered in this study are (i) LC-BLYP,[28] which appoints 100% of HFX at infinite distance and no HFX at zero distance, with $\alpha_1 = 0.0$, $\alpha_2 = 1.0$ and a standard value of the RS parameter (ω_{std}) of 0.47 Bohr^{-1}, (ii) CAM-B3LYP,[29] which uses the coulomb-attenuating method and includes 19% of HFX at short-range and 65% at long-range with $\alpha_1 = 0.19$, $\alpha_2 = 0.46$ and $\omega_{\mathrm{std}} = 0.33$ Bohr^{-1}, and (iii) ωB97XD,[30] which includes respectively 22.20% and 77.80% of HFX at short- and long-range, with $\alpha_1 = 0.222$, $\alpha_2 = 0.778$ and $\omega_{\mathrm{std}} = 0.20$ Bohr^{-1}. This last functional also incorporates empirical atom–atom dispersion corrections, though independent of applied external fields. In addition to calculations using standard values of the RS parameter, we carried out calculations using optimally-tuned ω values in order to obtain a more accurate description of CT excitation energies and NLO responses. The procedure used to determine optimal system-dependent ω values is described in the next subsection.

In addition to DFT, hyperpolarizabilities were calculated using the coupled-perturbed Hartree–Fock method (CPHF), as well as using the second-order Møller–Plesset perturbation theory (MP2) in combination with a finite field (FF) procedure. A fully automatized Romberg scheme was used to improve and control the accuracy of the numerical derivatives, using field amplitudes ranging from ±0.0008 to ±0.0032 a.u. for compounds with $n = 0$, and from ±0.0002 to ±0.0032 a.u. for compounds with $n = 1$–4.[31] Since the MP2 method was shown to closely reproduce the NLO responses obtained with reference CCSD(T) calculations for push–pull π-conjugated systems,[14] MP2 values are used as theoretical references in this study.

Solvent effects were included in both geometry optimizations and calculations of the optical properties by using the Integral Equation Formalism (IEF) version of the Polarizable Continuum Model (IEF-PCM).[32,33] In line with experimental characterizations, chloroform was used as solvent, with dielectric constants $\varepsilon_0 = 4.711$ in the static limit and $\varepsilon_\infty = 2.091$ at infinite frequency. All calculations were performed with the Gaussian16 package.[34]

2.2 Optimal tuning of the range separation parameters

The range-separation parameters ω were optimized according to a standard nonempirical system-specific procedure, such that Koopmans' theorem for both neutral and anion is obeyed as closely as possible.[35–38] Optimal ω values, denoted as ω_{opt} in the following, corresponds to the minimum of the function below, which is found using the golden-section search algorithm:[39]

$$J(\omega) = \sqrt{J_0^2(\omega) + J_1^2(\omega)} \quad (2)$$

where

$$J_0(\omega) = |\varepsilon_{\mathrm{HOMO}}(N) + \mathrm{IP}(N)| \quad (3)$$

$$J_1(\omega) = |\varepsilon_{\mathrm{HOMO}}(N+1) + \mathrm{EA}(N)| \quad (4)$$

$\varepsilon_{\mathrm{HOMO}}(N)$ and $\varepsilon_{\mathrm{HOMO}}(N+1)$ are the HOMO energies of the system with N (neutral) and $N+1$ electrons (anion), respectively. The ionization potential (IP) and electron affinity (EA) are calculated as the differences between ground-state energies of systems with N and $N \pm 1$ electrons:

$$\mathrm{IP}(N) = E(N-1) - E(N) \quad (5)$$

$$\mathrm{EA}(N) = \mathrm{IP}(N+1) = E(N) - E(N+1) \quad (6)$$

Two different ω-tuning schemes were employed, differing in the computation of IP and EA. In the first one, these two quantities are calculated using the standard attenuating parameter (ω_{std}) of the functional, so that their values are kept fixed throughout the optimization procedure. In the second one, IP and EA are calculated self-consistently, *i.e.* using the optimal value of the RS parameter (ω_{opt}) at each step of the process. This second procedure is the most common way of optimizing ω, but results in larger computational times. To the best of our knowledge, we report here the first study comparing the performance of self-consistent (SC) and non self-consistent (NSC) ω-tuning schemes.

While ω-tuning schemes were shown to provide improved fundamental gaps and absorption properties,[19,37,38,40–42] the conclusions are more controversial regarding second-order NLO responses. In recent studies, Sun and Autschbach,[19] as well as Scuseria and coworkers[20] concluded that LRC-XCFs using physically-adjusted RS parameters lead to improved description of the first hyperpolarizabilities of D–A-substituted organic molecules. Improved correlation with reference CCSD(T) second-hyperpolarizability values was also obtained by Matito, Luis *et al.* by empirically tuning the RS parameter of the LC-BLYP functional for a benchmark set of 60 medium-size molecules.[43] In contradiction, other investigations reported that the tuning of ω to enforce Koopmans' theorem does not offer real improvement in the description of NLO properties.[42,44] In this work, ω values were optimized in the gas phase for the LC-BLYP, CAM-B3LYP and ωB97XD LRC hybrids. Since it was also demonstrated in previous works that ω values optimized in solvent media using PCM provide reliable hyperpolarizabilities compared to experiments,[20] the ω values of the LC-BLYP functional were also optimized in the presence of a dielectric continuum.

2.3 Nonlinear optical properties

The NLO quantities under scrutiny are related to HRS experiments. For a non-polarized incident light of frequency ω, the intensity of the vertically polarized (parallel to the Z axis of the laboratory frame) SHG signal, scattered at 90° with respect to the propagation direction (parallel to the Y axis), is proportional to the square of the

HRS hyperpolarizability:

$$\beta_{HRS}(-2\omega;\omega,\omega) = \beta_{HRS} = \sqrt{\langle \beta_{HRS}{}^2 \rangle} = \sqrt{\langle \beta_{ZZZ}{}^2 \rangle + \langle \beta_{ZXX}{}^2 \rangle} \quad (7)$$

where $\langle \beta_{ZZZ}{}^2 \rangle$ and $\langle \beta_{ZXX}{}^2 \rangle$ are averages of β tensor components that describe the isotropic distribution of molecular orientations in dilute solutions:

$$\begin{aligned}\langle \beta_{ZZZ}{}^2 \rangle = {} & \frac{1}{7}\sum_{\zeta}^{x,y,z} \beta_{\zeta\zeta\zeta}{}^2 + \frac{4}{35}\sum_{\zeta\neq\eta}^{x,y,z} \beta_{\zeta\zeta\eta}{}^2 + \frac{2}{35}\sum_{\zeta\neq\eta}^{x,y,z} \beta_{\zeta\zeta\zeta}\beta_{\zeta\eta\eta} \\ & + \frac{4}{35}\sum_{\zeta\neq\eta}^{x,y,z} \beta_{\eta\zeta\zeta}\beta_{\zeta\zeta\eta} + \frac{4}{35}\sum_{\zeta\neq\eta}^{x,y,z} \beta_{\zeta\zeta\zeta}\beta_{\eta\eta\zeta} + \frac{1}{35}\sum_{\zeta\neq\eta}^{x,y,z} \beta_{\eta\zeta\zeta}{}^2 \\ & + \frac{4}{105}\sum_{\zeta\neq\eta\neq\xi}^{x,y,z} \beta_{\zeta\zeta\eta}\beta_{\eta\xi\xi} + \frac{1}{105}\sum_{\zeta\neq\eta\neq\xi}^{x,y,z} \beta_{\eta\zeta\zeta}\beta_{\eta\xi\xi} \\ & + \frac{4}{105}\sum_{\zeta\neq\eta\neq\xi}^{x,y,z} \beta_{\zeta\zeta\eta}\beta_{\xi\xi\eta} + \frac{2}{105}\sum_{\zeta\neq\eta\neq\xi}^{x,y,z} \beta_{\zeta\eta\xi}{}^2 \\ & + \frac{4}{105}\sum_{\zeta\neq\eta\neq\xi}^{x,y,z} \beta_{\zeta\eta\xi}\beta_{\eta\zeta\xi}\end{aligned} \quad (8)$$

$$\begin{aligned}\langle \beta_{ZXX}{}^2 \rangle = {} & \frac{1}{35}\sum_{\zeta}^{x,y,z} \beta_{\zeta\zeta\zeta}{}^2 + \frac{4}{105}\sum_{\zeta\neq\eta}^{x,y,z} \beta_{\zeta\zeta\zeta}\beta_{\zeta\eta\eta} - \frac{2}{35}\sum_{\zeta\neq\eta}^{x,y,z} \beta_{\zeta\zeta\zeta}\beta_{\eta\eta\zeta} \\ & + \frac{8}{105}\sum_{\zeta\neq\eta}^{x,y,z} \beta_{\zeta\zeta\eta}{}^2 + \frac{3}{35}\sum_{\zeta\neq\eta}^{x,y,z} \beta_{\zeta\eta\eta}{}^2 - \frac{2}{35}\sum_{\zeta\neq\eta}^{x,y,z} \beta_{\zeta\zeta\eta}\beta_{\eta\zeta\zeta} \\ & + \frac{1}{35}\sum_{\zeta\neq\eta\neq\xi}^{x,y,z} \beta_{\zeta\eta\eta}\beta_{\zeta\xi\xi} - \frac{2}{105}\sum_{\zeta\neq\eta\neq\xi}^{x,y,z} \beta_{\zeta\zeta\xi}\beta_{\eta\eta\xi} \\ & - \frac{2}{105}\sum_{\zeta\neq\eta\neq\xi}^{x,y,z} \beta_{\zeta\zeta\eta}\beta_{\eta\xi\xi} + \frac{2}{35}\sum_{\zeta\neq\eta\neq\xi}^{x,y,z} \beta_{\zeta\eta\xi}{}^2 \\ & - \frac{2}{105}\sum_{\zeta\neq\eta\neq\xi}^{x,y,z} \beta_{\zeta\eta\xi}\beta_{\eta\zeta\xi}\end{aligned} \quad (9)$$

where {*x*,*y*,*z*} are the axes of the molecular frame. In line with experimental characterizations, the dynamic (frequency-dependent) β tensor components were calculated using an infrared incident wavelength (photon energy) of 1907 nm (0.65 eV). The reported values are given in atomic units (1 a.u. of β = 3.6310 × 10^{-42} m^4 V^{-1} = 3.2063 × 10^{-53} C^3 m^3 J^{-2} = 8.641 × 10^{-33} esu) in the T convention, which assumes a Taylor series expansion of the electric molecular dipoles as a function of the applied electric fields.[45] In addition to β_{HRS}, the depolarization ratios (DR = $\langle \beta_{ZZZ}{}^2 \rangle / \langle \beta_{ZXX}{}^2 \rangle$) were also calculated as indicators of the symmetry of the NLO response of the chromophores.

In the following, the HRS hyperpolarizabilities of the investigated systems are rationalized by relying on the two-state approximation (TSA), which assumes that only one electronic excited state (here the S_1 state) contributes to the sum-over-state expression of the second-order NLO response:[46]

$$\beta_{HRS}^{TSA} = 9\sqrt{\frac{6}{35}} \times \frac{f_{01}\Delta\mu_{01}}{\Delta E_{01}{}^3} \times \left| F_{disp}^{TSA} \right| \quad (10)$$

with:

$$F_{disp}^{TSA} = \frac{\Delta E_{01}{}^4}{(\Delta E_{01}{}^2 - (\hbar\omega)^2)(\Delta E_{01}{}^2 - (2\hbar\omega)^2)} \quad (11)$$

where ΔE_{01} is the $S_0 \rightarrow S_1$ excitation energy, f_{01} is the associated oscillator strength, and $\Delta\mu_{01} = ||\vec{\mu}_{S_1} - \vec{\mu}_{S_0}||$ is the dipole moment variation between the two electronic states. To gain deeper insight on the origin of the light-induced intramolecular charge transfer (ICT), $\Delta\mu_{01}$ is further decomposed as the product of the photo-induced charge displacement (Δq_{01}) and charge transfer distance (Δr_{01}): $\Delta\mu_{01} = \Delta q_{01} \times \Delta r_{01}$.[47,48] $F^{TSA}(\omega)$ is the frequency dispersion factor, with $\hbar\omega$ the photon energy of the incident beam (0.65 eV). From eqn (11), F_{disp}^{TSA} is equal to 1 in the static limit ($\hbar\omega = 0$), to ~0.5 if $\hbar\omega = \Delta E_{01}/3$, and tends to infinite in the resonance limit ($\hbar\omega = \Delta E_{01}/2$).

2.4 Experimental reference data

Experimental UV/vis data as well as HRS hyperpolarizabilities measured in chloroform using an incident wavelength of 1907 nm are gathered in Table 1. Experimental β_{HRS} values are given according convention T, and are relative to the HRS response of the DR1 reference molecule provided in ref. 49 (see also note ref. 50). Static first hyperpolarizabilities (*i.e.* at infinite wavelength) were extrapolated from the dynamic ones according to the two-state model, after introducing a homogeneous damping Γ into the frequency dispersion factor (eqn (11)) to attenuate the resonance effects:

$$\begin{aligned} F_{disp}^{TSA}(\Gamma) &= \frac{\beta_{HRS}^{1907}}{\beta_{HRS}^{\infty}} \\ &= \frac{\Delta E_{01}{}^2(\Delta E_{01} - i\Gamma)^2}{\left\{(\Delta E_{01} - i\Gamma)^2 - (\hbar\omega)^2\right\}\left\{(\Delta E_{01} - i\Gamma)^2 - (2\hbar\omega)^2\right\}} \end{aligned} \quad (12)$$

In line with previous studies including a previous report on these derivatives,[23,51–53] the static first hyperpolarizabilities were extrapolated by setting Γ to 1.2 times the half width at half maximum (HWHM) of the first absorption band (Table 1), in order to account for the change in the absorption bandwidth from one compound to another. For comparison, β_{HRS}^{∞} values were also extrapolated in the absence of homogeneous damping (Γ = 0).

3 Results and discussion

3.1 Molecular structures

As mentioned above, reliable predictions of the optical properties of π-conjugated systems require an accurate description of the geometrical parameters associated to the electronic

Table 1 Experimental data (all measured in chloroform) used as references for calculations.[21,23] Maximal absorption wavelengths (λ_{max}, nm), half widths at half maximum (HWHM, cm^{-1}) of the main absorption band, dynamic first hyperpolarizabilities (β^{1907}_{HRS}, a.u.), and static ones extrapolated using eqn (12) with Γ = 0 ($\beta^{\infty}_{HRS}(0)$, a.u.) and Γ = 1.2 × HWHM ($\beta^{\infty}_{HRS}(\Gamma)$, a.u.). Relative $\beta[n]/\beta[0]$ values are reported in parentheses for each series of compounds

	λ_{max}	HWHM	β^{1907}_{HRS}	$F^{TSA}_{disp}(0)$	$\beta^{\infty}_{HRS}(0)$	$F^{TSA}_{disp}(\Gamma)$	$\beta^{\infty}_{HRS}(\Gamma)$
I[0]	470	1700	5800 (1.0)	1.41	4140 (1.0)	1.38	4220 (1.0)
I[1]	529	2350	9190 (1.6)	1.56	5852 (1.4)	1.47	6270 (1.5)
I[2]	565	2550	17 900 (3.1)	1.69	10 570 (2.6)	1.53	11 660 (2.8)
I′[0]	515	950	8710 (1.0)	1.52	5730 (1.0)	1.51	5770 (1.0)
I′[1]	614	850	10 640 (1.2)	1.91	5601 (1.0)	1.87	5680 (1.0)
I′[2]	704	1500	24 670 (2.8)	2.54	9700 (1.7)	2.27	10 870 (1.9)
I′[3]	712	2250	71 590 (8.2)	2.62	27 250 (4.8)	2.04	35 070 (6.1)
I′[4]	720	2550	418 430 (48.1)	2.71	154 330 (27.0)	1.95	214 220 (37.1)
II[0]	566	1100	21 280 (1.0)	1.69	12 580 (1.0)	1.66	12 830 (1.0)
II[1]	668	1025	27 090 (1.3)	2.24	12 120 (1.0)	2.15	12 620 (1.0)
II[2]	759	1400	277 670 (13.0)	3.24	85 690 (6.8)	2.71	102 280 (8.0)
II′[0]	581	650	22 740 (1.0)	1.75	12 960 (1.0)	1.74	13 080 (1.0)
II′[1]	690	450	37 730 (1.7)	2.41	15 630 (1.2)	2.39	15 800 (1.2)
II′[2]	803	415	304 760 (13.4)	4.18	72 980 (5.6)	4.04	75 410 (5.8)
II′[3]	916	400	1 886 590 (83.0)	16.77	112 530 (8.7)	11.19	168 620 (12.9)

delocalization along the molecular backbone, in particular the bond length alternation (BLA). BLA values were calculated at the IEFPCM:M06-2X/6-311G(d) level for the four series of derivatives, according to the following expression:

$$\mathrm{BLA} = \frac{1}{2n+1}\sum_{i=1}^{N-2}(-1)^{i+1} \times (d_{i+1} - d_i) \qquad (13)$$

where d_i is the ith interatomic distance within the polyenic linker of length n connecting the donor and acceptor units (see Fig. S1 and Table S1, ESI†). Note that this expression provides BLA values that are negative for all compounds. For simplicity, only the amplitudes are reported in the following.

As shown in Fig. 2, the evolution of BLA with chain length differs from one series to another. In compounds incorporating a dimethylaminophenyl as donor group (**I[*n*]** and **II[*n*]**), BLA values display small variations with n, with values ranging from 0.066 to 0.074 Å for **I[*n*]** and from 0.052 to 0.064 Å for **II[*n*]**. In series **I′[*n*]** and **II′[*n*]** that include a dimethylaminothiophene donor, BLA values show much larger variations (from 0.024 to 0.067 Å for **I′[*n*]**, and from 0.002 to 0.054 Å for **II′[*n*]**). Consistently with the decrease of the π-electron conjugation with respect to increasing n, the pyramidalization angle of the dimethylamino substituent increases, as reported in Table S2 (ESI†).

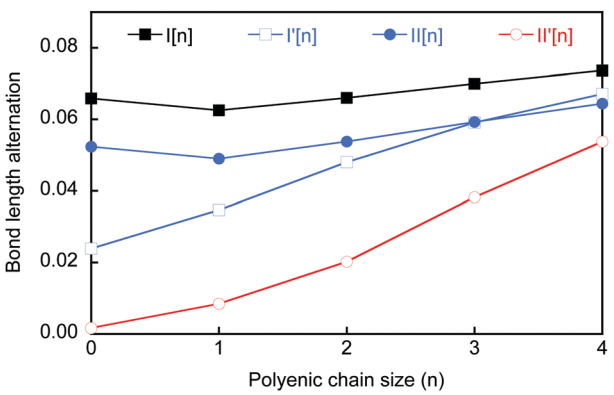

Fig. 2 Bond length alternation (in Å) calculated along the polyenic bridge of the four series of derivatives at the IEFPCM:M06-2X/6-311G(d) in chloroform.

3.2 Static first hyperpolarizabilities

3.2.1 Reference *ab initio* calculations. Table 2 reports the static HRS hyperpolarizability of the four merocyanine series calculated at the CPHF and MP2 levels. Previous theoretical investigations demonstrated that the MP2 level, as a result of cancellations between higher-order contributions, includes the largest part of electron correlation effects and closely reproduces the first hyperpolarizability of push–pull π-conjugated systems obtained with the CCSD(T) scheme.[14] β^{MP2}_{HRS} values are thus used as theoretical references in the following, while comparison to β^{CPHF}_{HRS} values provides a direct measure of the magnitude of electron correlation effects.

As expected from previous works,[10,13,14,31,53,54] electron correlation enhances the first hyperpolarizability by a factor ranging between 1.97 and 3.43. The $\beta^{MP2}_{HRS}/\beta^{CPHF}_{HRS}$ ratio is system-dependent, which demonstrates the need of including electron correlation effects since the latter introduce a non systematic scaling of the β_{HRS} values that might impact qualitative interpretations. As shown in Fig. 3, the $\beta^{MP2}_{HRS}/\beta^{CPHF}_{HRS}$ ratios smoothly increase with the size n of the polyenic bridge up to a maximum value obtained for n = 3, and then slightly decrease. Although it follows the same trend, the **II′[*n*]** series, which incorporates the strongest D/A pair, displays stronger variations of the $\beta^{MP2}_{HRS}/\beta^{CPHF}_{HRS}$ ratio as a function of n.

As reported in Tables S25 and S26 (ESI†), the computed depolarization ratios are typical of one-dimensional push–pull π-conjugated systems; they range from 4.0 to 4.8 at the HF level, and are systematically larger (from 4.5 to 5.0) when introducing electron correlation effects at the MP2 level. Noteworthy, both levels of calculation evidence that increasing the conjugation length from n = 0 to n = 4 within a molecular series reinforces

Table 2 Static HRS hyperpolarizabilities (β^{∞}_{HRS}, a.u.) and relative $\beta^{\infty}_{HRS}[n]/\beta^{\infty}_{HRS}[0]$ values calculated at the CPHF/6-311+G(d) and MP2/6-311+G(d) levels in chloroform

	CPHF		MP2	
	β^{∞}_{HRS}	$\beta^{\infty}_{HRS}[n]/\beta^{\infty}_{HRS}[0]$	β^{∞}_{HRS}	$\beta^{\infty}_{HRS}[n]/\beta^{\infty}_{HRS}[0]$
I[0]	4372	1.0	9797	1.0
I[1]	9530	2.2	24 979	2.5
I[2]	16 782	3.8	47 273	4.8
I[3]	25 344	5.8	72 384	7.4
I[4]	33 739	7.7	94 967	9.7
I′[0]	3917	1.0	8299	1.0
I′[1]	11 120	2.8	29 722	3.6
I′[2]	24 024	6.1	71 680	8.6
I′[3]	35 675	9.1	106 571	12.8
I′[4]	42 662	10.9	123 604	14.9
II[0]	7173	1.0	17 364	1.0
II[1]	15 553	2.2	43 885	2.5
II[2]	27 055	3.8	82 765	4.8
II[3]	40 143	5.6	125 463	7.2
II[4]	53 090	7.4	163 570	9.4
II′[0]	5587	1.0	10 982	1.0
II′[1]	13 591	2.4	32 228	2.9
II′[2]	35 754	6.4	112 592	10.3
II′[3]	67 724	12.1	232 020	21.1
II′[4]	76 914	13.8	250 702	22.8

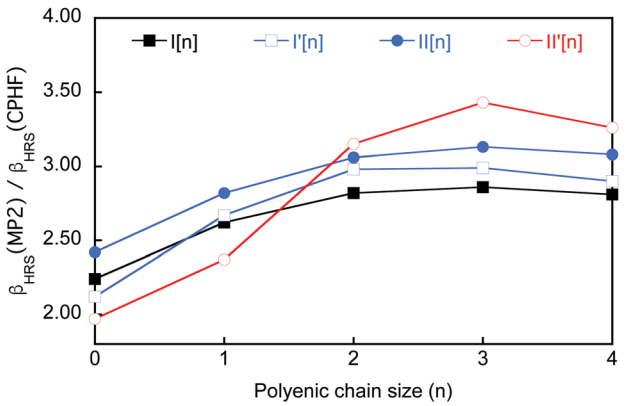

Fig. 3 $\beta^{MP2}_{HRS}/\beta^{CPHF}_{HRS}$ ratio as a function of chain length in the four series of derivatives.

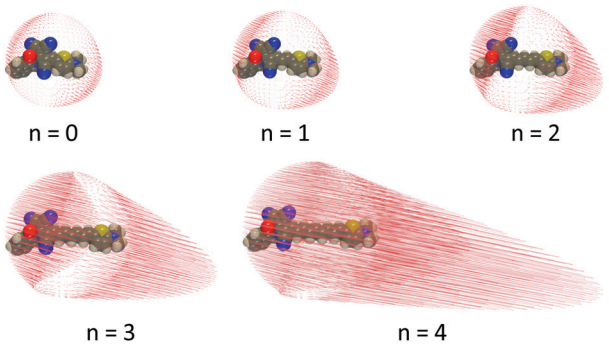

Fig. 4 Unit sphere representation of the static first hyperpolarizability tensor for compounds **II′[*n*]** (n = 0–4), as calculated at the CPHF level.[56]

the 1D character of the NLO response, as also highlighted by unit sphere representations[55] of the β tensor (see Fig. 4 for the **II′[*n*]** series).

3.2.2 Two-state approximation. We address in this section the reliability of the two-state approximation, by comparing the static β^{TSA}_{HRS} values calculated using eqn (10) with those calculated using full-featured CPHF calculations (β^{CPHF}_{HRS}). As shown in Fig. 5a, the two sets of values correlate well (with correlation coefficients $R^2 \geq 0.99$, see Table S43, ESI†), which proves the suitability of the TSA for describing qualitatively the variations of β_{HRS}. Note that the correlation remains very good (R^2 = 0.986) when considering the four series of molecules altogether (Fig. S11, ESI†). However, as illustrated in Fig. 5b for the four series of compounds, the relative error is not systematic, the TSA providing underestimated β_{HRS} values for small molecules, and overestimated ones for larger compounds. Besides, large relative errors (ranging between 40% and 46%) are obtained for the largest systems (n = 4). The same conclusions hold when the first hyperpolarizabilities are computed at the Coupled-Perturbed Kohn–Sham (CPKS) level. Interestingly, varying the XC functional within a given series of compounds does not induce significant changes in the evolution of β^{TSA}_{HRS} with respect to β^{CPKS}_{HRS}, and gives rise to linear regression equations with very similar slope coefficients (Table S43, ESI†). This indicates that the evolution of the error made on the HRS hyperpolarizabilities when using the TSA (see also Tables S41 and S42, ESI†) hardly depends on the level of calculation, which further confirms the robustness of the two-state approximation for qualitative interpretations.

3.2.3 Effect of the amount of exact HF exchange. The static HRS hyperpolarizabilities calculated using the Minnesota family of XCFs are collected in Table 3 for the four series of compounds. We first discuss the evolution of β^{∞}_{HRS} with respect to the percentage of HF exchange (%HFX) included in the functional for a given compound. As shown in Fig. 6, β^{∞}_{HRS} of shorter derivatives hardly depends on %HFX, while it has a strong impact for the larger ones, since the latter are more affected by conjugation effects.[57] In series incorporating a dimethylaminophenyl as donor group (**I[*n*]** and **II[*n*]**), β^{∞}_{HRS} linearly decreases with %HFX, as previously reported for other extended NLO chromophores.[17] The series **I′[*n*]** and **II′[*n*]** that include a dimethylaminothiophene donor exhibit a less usual behavior: β^{∞}_{HRS} linearly increases with %HFX for shorter compounds (n = 0–2), whereas it evolves non monotonically for **I′[3]** and **II′[4]**, for which a maximum is found for %HFX = 54% (M06-2X). In the case of **I′[4]**, β^{∞}_{HRS} displays a slightly marked maximum for a lower amount of HF exchange (%HFX = 27%), corresponding to the M06 functional.

These different behaviors can be rationalized by analyzing the independent evolution of the spectroscopic quantities entering in the two-state expression of β^{∞}_{HRS} (eqn (10)). As shown in Fig. S3 and S5 (ESI†), the first charge-transfer excitation energy (ΔE_{01}) linearly increases with %HFX in the **I[*n*]** and **II[*n*]** series, as a result of the increase of the HOMO–LUMO gap. With few exceptions, the dipole moment variation between the ground and first

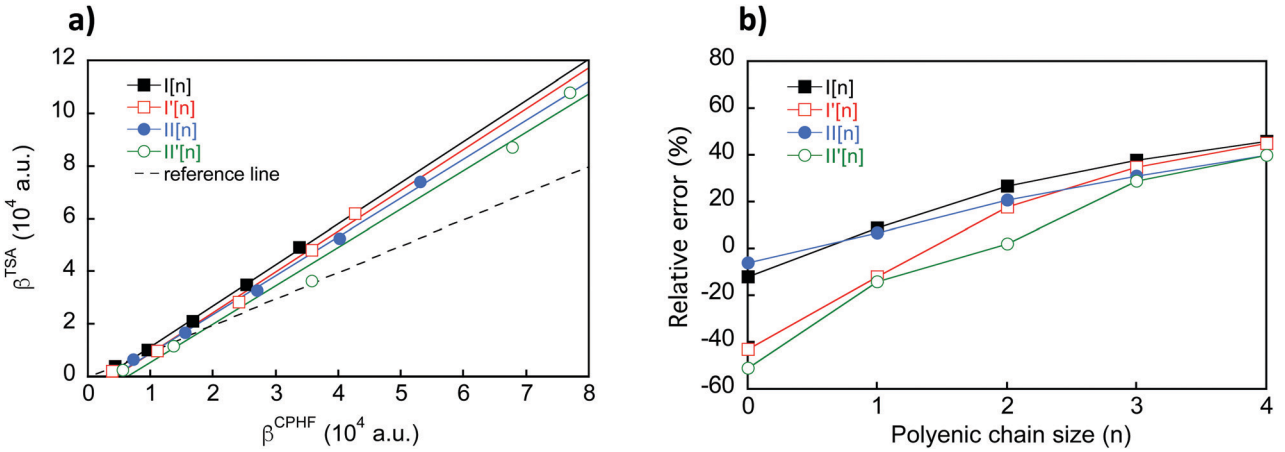

Fig. 5 (a) Static β_{HRS} values of the four merocyanine series evaluated using the two-state approximation, plotted against the values calculated using CPHF/6-311+G(d) calculations in chloroform. Lines are linear fits. (b) Evolution of the relative error (defined as Err = $(\beta_{HRS}^{TSA} - \beta_{HRS}^{CPHF})/\beta_{HRS}^{CPHF} \times 100$) with the length of the polyenic bridge.

Table 3 Static HRS hyperpolarizabilities (β_{HRS}^{∞}, a.u.) and relative $\beta_{HRS}^{\infty}[n]/\beta_{HRS}^{\infty}[0]$ values calculated in chloroform using the M06 series of XCFs in combination with the 6-311+G(d) basis set

	M06L		M06		M06-2X		M06-HF	
	β_{HRS}^{∞}	$\beta[n]/\beta[0]$	β_{HRS}^{∞}	$\beta[n]/\beta[0]$	β_{HRS}^{∞}	$\beta[n]/\beta[0]$	β_{HRS}^{∞}	$\beta[n]/\beta[0]$
I[0]	7800	1.0	7331	1.0	7550	1.0	7215	1.0
I[1]	19 261	2.5	18 431	2.5	19 104	2.5	17 318	2.4
I[2]	42 325	5.4	39 177	5.3	38 422	5.1	30 792	4.3
I[3]	84 258	10.8	72 671	9.9	64 572	8.6	44 320	6.1
I[4]	154 269	19.8	120 043	16.4	94 611	12.5	55 179	7.6
I′[0]	4529	1.0	4832	1.0	5676	1.0	6730	1.0
I′[1]	11 033	2.4	12 869	2.7	16 829	3.0	22 388	3.3
I′[2]	27 713	6.1	33 115	6.9	42 661	7.5	48 973	7.3
I′[3]	63 288	14.0	71 646	14.8	80 109	14.1	66 169	9.8
I′[4]	128 361	28.3	128 759	26.6	117 205	20.7	71 644	10.6
II[0]	13 021	1.0	12 522	1.0	12 766	1.0	12 435	1.0
II[1]	29 405	2.3	29 581	2.4	31 297	2.5	30 440	2.4
II[2]	61 853	4.8	61 284	4.9	62 881	4.9	54 822	4.4
II[3]	120 983	9.3	113 035	9.0	106 273	8.3	78 372	6.3
II[4]	223 158	17.1	190 547	15.2	157 463	12.3	96 263	7.7
II′[0]	5836	1.0	6476	1.0	7272	1.0	8769	1.0
II′[1]	11 525	2.0	13 773	2.1	17 496	2.4	25 773	2.9
II′[2]	26 435	4.5	33 966	5.2	49 182	6.8	87 460	10.0
II′[3]	69 848	12.0	90 972	14.0	126 131	17.3	158 799	18.1
II′[4]	162 471	27.8	192 302	29.7	208 061	28.6	150 724	17.2

dipole-allowed CT state ($\Delta\mu_{01}$) also increases linearly for shorter compounds (n = 0–2), while the variation becomes non monotonic for **I[3]**, **I[4]** and **II[4]**. Combined with the saturation of the oscillator strengths, these different behaviors result in the regular decrease of β_{HRS}^{∞} with %HFX in these two series. The unexpected increase of β_{HRS}^{∞} observed for the shortest compounds in the **I′[*n*]** and **II′[*n*]** series mainly originates from the weak dependence of ΔE_{01} on %HFX (Fig. S4 and S6, ESI†), while $\Delta\mu_{01}$ and f_{01} globally increase. In derivatives with longer polyenic chains, ΔE_{01} displays a more pronounced increase with %HFX, which translates into the lowering of β_{HRS}^{∞}.

It is also informative to compare the evolution with chain length of β_{HRS}^{∞} obtained using the Minnesota functionals and the evolution obtained at the CPHF and MP2 levels (Fig. 7). For series **I[*n*]** and **II[*n*]**, the M06L and M06 XCFs overestimate the size effects and significantly deviate from MP2 reference results for larger compounds. This behavior is consistent with previous investigations that have reported the nearly catastrophic evolution of mild hybrid XCFs with respect to increasing the conjugation length.[16,18–20] Reversely, M06-HF closely follows the size evolution obtained at the CPHF level, as expected owing to the fact that β_{HRS}^{∞} values are hardly impacted by the correlation part of the functional. Nevertheless, one notes that the CPHF and M06-HF β_{HRS}^{∞} values are significantly different, possibly due to the kinetic energy functional. As also shown in previous works,[17] M06-2X closely reproduces the results obtained at the MP2 level, demonstrating that this XCF incorporates the adequate balance between DFT and HF exchange for computing the NLO properties in conjugated push–pull chromophores.

The situation is more complex for series **I′[*n*]** and **II′[*n*]**. Both CPHF and MP2 β_{HRS}^{∞} values show a saturation for long chains, which is more pronounced for **II′[*n*]**. This behavior is reproduced only by M06-HF, the other XCFs (including M06-2X) showing a monotonic increase of the static first hyperpolarizability. The difference in the evolution of β_{HRS}^{∞} with system size between series including a dimethylaminophenyl and those including a dimethylaminothiophenyl can be directly ascribed to the difference in the evolution of the bond length alternation (Fig. 2), and qualitatively interpreted using a two-form model mixing neutral and zwitterionic forms.[58–60] In this model, the evolution of β_{HRS}^{∞} with BLA exhibits a peak between the polyene and the cyanine limits, crosses through zero at the cyanine limit (where BLA = 0), and exhibits another peak between the cyanine and zwitterionic limits. Whereas the BLA hardly changes with n in series **I[*n*]** and **II[*n*]**, it strongly increases in series **I′[*n*]** and **II′[*n*]**, starting closer to the cyanine limit in the case of **II′[0]**. When increasing n in the latter series, the BLA increases and shifts the two-form equilibrium close to

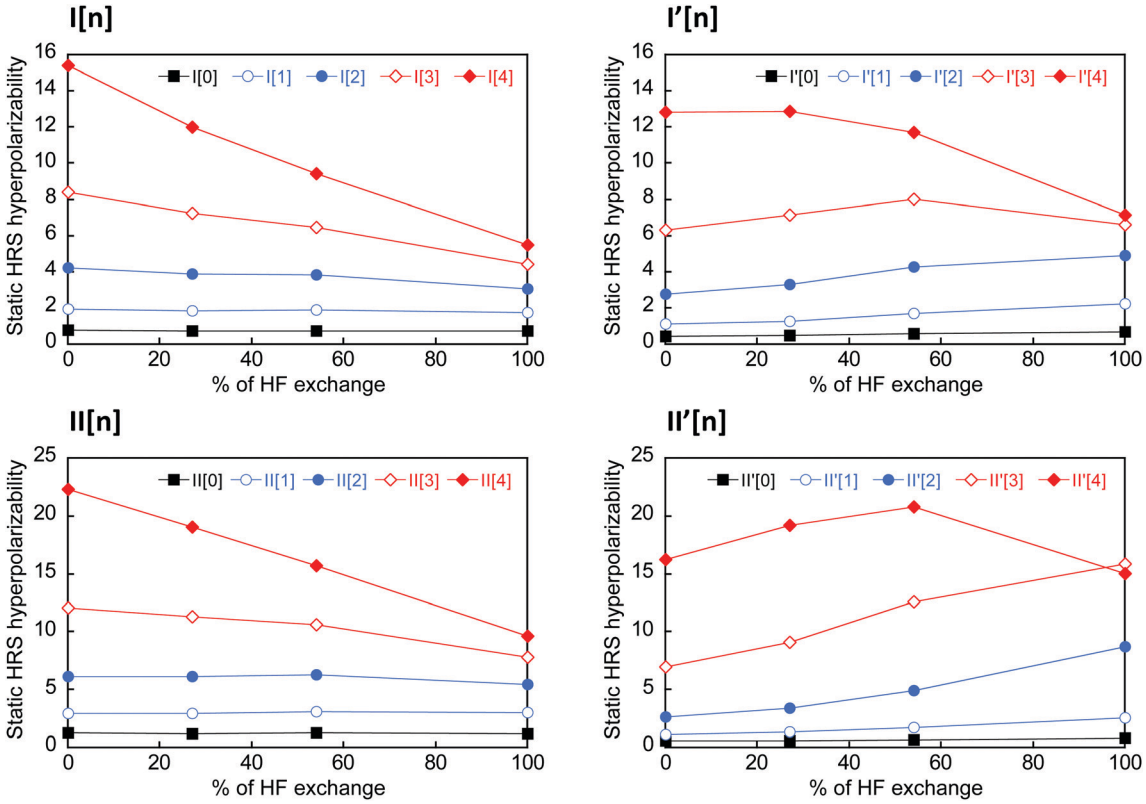

Fig. 6 Static HRS hyperpolarizabilities (in 10^4 a.u.) of the four series of merocyanines, calculated in chloroform using the Minnesota's family of functionals (M06L, M06, M06-2X, M06-HF) in combination with the 6-311+G(d) basis set. Results are reported as a function of the percentage of HF exchange included in the XCF.

the polyene limit, where β_{HRS}^{∞} saturates before reaching its maximum value.

3.2.4 Optimal tuning of the range-separation parameter in RS-XCFs. Optimal values of the RS parameters obtained in the gas phase using the self-consistent (SC) and non-self-consistent (NSC) optimization schemes (see Section 2.2) are collected in Table S3a (ESI†) for the four series of merocyanines. The differences in the ω_{opt} values obtained using the two tuning schemes, as well as the induced differences on the optical properties of the investigated compounds, are discussed in detail in the ESI† and illustrated in Fig. S7. Summarizing the main findings, for a given functional, SC and NSC optimization schemes provide close optimal ω values and similar evolution of the first hyperpolarizabilities with chain length. Nevertheless, the accuracy of the NSC scheme with respect to the SC one depends on the choice of the XCF. Significant differences in the β_{HRS} values computed using the two procedures were notably obtained with LC-BLYP, where deviations can reach 15% and 20% for static and dynamic β_{HRS}, respectively. From now on, only properties computed using the self-consistent method will be discussed.

For LC-BLYP and ωB97XD, the optimally-tuned ω values are comprised in the ranges 0.16–0.20 $Bohr^{-1}$ and 0.11–0.15 $Bohr^{-1}$, respectively, both smaller than the standard ω values. Conversely, ω values optimized for CAM-B3LYP are larger than ω_{std} and range between 0.41 and 0.95 $Bohr^{-1}$. As mentioned in earlier works,[19,37,38,40,42,61] ω_{opt} decreases for all XCFs when increasing the system size. Whatever the functional, the variation of ω_{opt} with chain length is larger for series **I**[*n*] and **II**[*n*] than for series **I′**[*n*] and **II′**[*n*]. For a given molecular family, ω values optimized for LC-BLYP and ωB97XD display much smaller variations with the system size than CAM-B3LYP, as previously reported by Garret *et al.* for other organic chromophores.[42]

Table 4 reports the β_{HRS}^{∞} values calculated at the LC-BLYP, ωB97XD and CAM-B3LYP level using default and optimally-tuned ω values. The evolution of β_{HRS}^{∞} with chain length is illustrated in Fig. 8 for the four families of merocyanines. If one excepts some results calculated with LC-BLYP and ω_{opt} for the larger compounds, the static hyperpolarizabilities computed using LRC functionals globally lie in between values computed at the CPHF and MP2 levels. β_{HRS}^{∞} values computed using LC-BLYP and ωB97XD with optimally-tuned RS parameters are quite similar, while they differ more significantly when using the default ω values (in part because ω values are getting more similar after optimization).

In series **I**[*n*] and **II**[*n*], the static hyperpolarizabilities computed using LC-BLYP and ωB97XD with optimally-tuned RS parameters are closer to reference MP2 results than those obtained using default ω values. This originates from the fact that $\omega_{opt} < \omega_{std}$, so that the fraction of HFX in those two XCFs is smaller after ω optimization, which increases the β_{HRS}^{∞} values. However, optimally-tuned LC-BLYP and ωB97XD

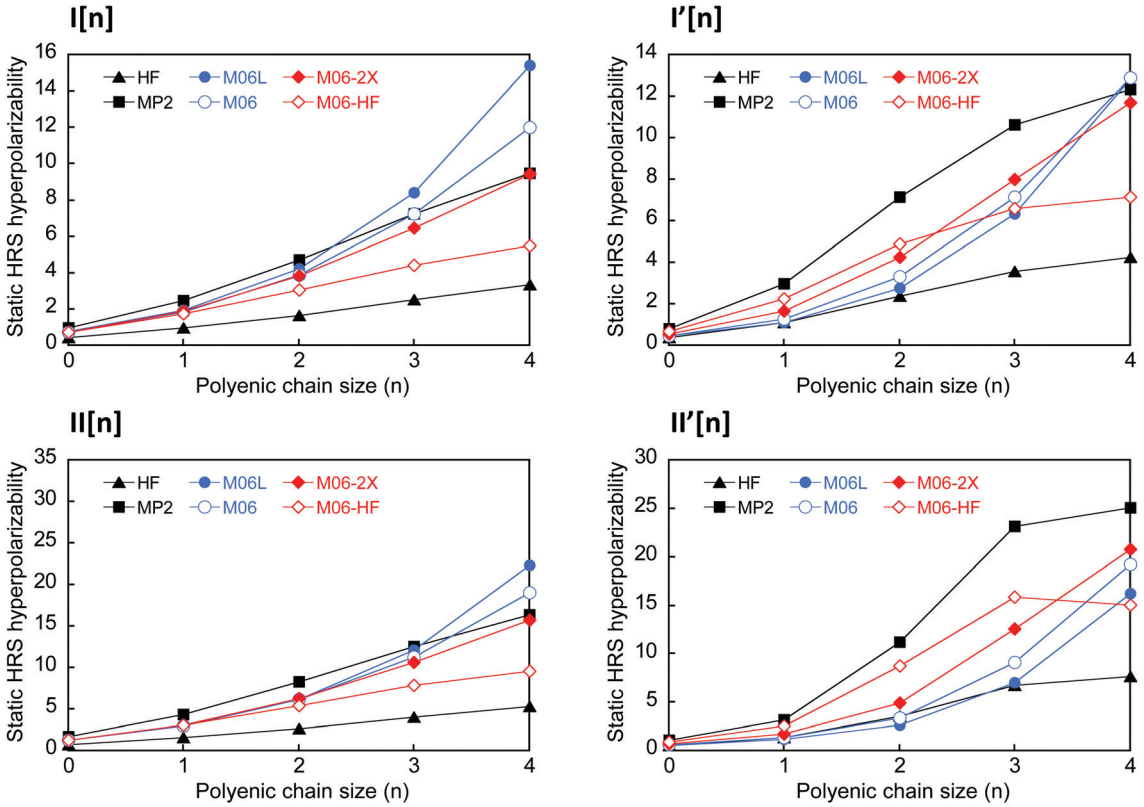

Fig. 7 Evolution of the static HRS hyperpolarizabilities (in 10^4 a.u.) with the length of the polyenic bridge in the four series of merocyanines, calculated in chloroform at the HF, MP2 and DFT levels using Minnesota's family of functionals in combination with the 6-311+G(d) basis set.

Table 4 Static HRS hyperpolarizabilities (β^{∞}_{HRS}, a.u.) and relative $\beta^{\infty}_{HRS}[n]/\beta^{\infty}_{HRS}[0]$ values calculated in chloroform using RS-XCFs in combination with the 6-311+G(d) basis set, using standard (ω_{std}) and optimally-tuned (ω_{opt}) RS parameters

	LC-BLYP				ωB97XD				CAM-B3LYP			
	ω_{std}		ω_{opt}		ω_{std}		ω_{opt}		ω_{std}		ω_{opt}	
I[0]	6703	1.0	7770	1.0	6964	1.0	7178	1.0	7159	1.0	6157	1.0
I[1]	16 121	2.4	19 818	2.6	17 263	2.5	18 079	2.5	17 943	2.5	15 418	2.5
I[2]	28 744	4.3	40 508	5.2	33 452	4.8	36 778	5.1	35 769	5.0	30 692	5.0
I[3]	41 654	6.2	69 994	9.0	53 769	7.7	63 309	8.8	59 596	8.3	5847	8.3
I[4]	52 244	7.8	106 174	13.7	74 881	10.8	95 694	13.3	86 062	12.0	72 699	11.8
I′[0]	6068	1.0	5630	1.0	5346	1.0	5166	1.0	5335	1.0	4815	1.0
I′[1]	19 971	3.3	16 146	2.9	16 101	3.0	14 743	2.9	15 762	3.0	15 142	3.1
I′[2]	43 944	7.2	41 454	7.4	40 318	7.5	37 859	7.3	40 058	7.5	38 600	8.0
I′[3]	60 735	10.0	82 071	14.6	71 132	13.3	74 817	14.5	74 530	14.0	68 981	14.3
I′[4]	67 029	11.0	128 900	22.9	96 112	18.0	116 851	22.6	107 262	20.1	94 970	19.7
II[0]	11 408	1.0	13 295	1.0	11 775	1.0	12 295	1.0	12 148	1.0	11 105	1.0
II[1]	27 817	2.4	32 548	2.4	28 631	2.4	29 732	2.4	29 551	2.4	27 460	2.5
II[2]	50 036	4.4	66 785	5.0	55 580	4.7	60 259	4.9	58 774	4.8	54 520	4.9
II[3]	71 721	6.3	117 219	8.8	89 194	7.6	104 703	8.5	98 087	8.1	90 140	8.1
II[4]	88 713	7.8	183 070	13.8	124 654	10.6	162 191	13.2	143 376	11.8	129 897	11.7
II′[0]	8113	1.0	7142	1.0	7162	1.0	6692	1.0	6976	1.0	6822	1.0
II′[1]	23 511	2.9	15 899	2.2	17 700	2.5	14 988	2.2	16 543	2.4	16 873	2.5
II′[2]	75 923	9.4	42 440	5.9	51 012	7.1	39 570	5.9	46 665	6.7	48 615	7.1
II′[3]	137 749	17.0	115 381	16.2	123 406	17.2	106 369	15.9	119 329	17.1	121 414	17.8
II′[4]	135 183	16.7	218 829	30.6	177 326	24.8	197 960	29.6	191 549	27.5	184 919	27.1

functionals overestimate the enhancement of the first hyperpolarizability with chain length compared to MP2. The situation is reversed in the case of CAM-B3LYP, for which ω-tuning increases the part of HFX in the XCF. In this case, β^{∞}_{HRS} values calculated using default ω are closer to MP2 references. Moreover, the increase of β^{∞}_{HRS} values with n is better reproduced.

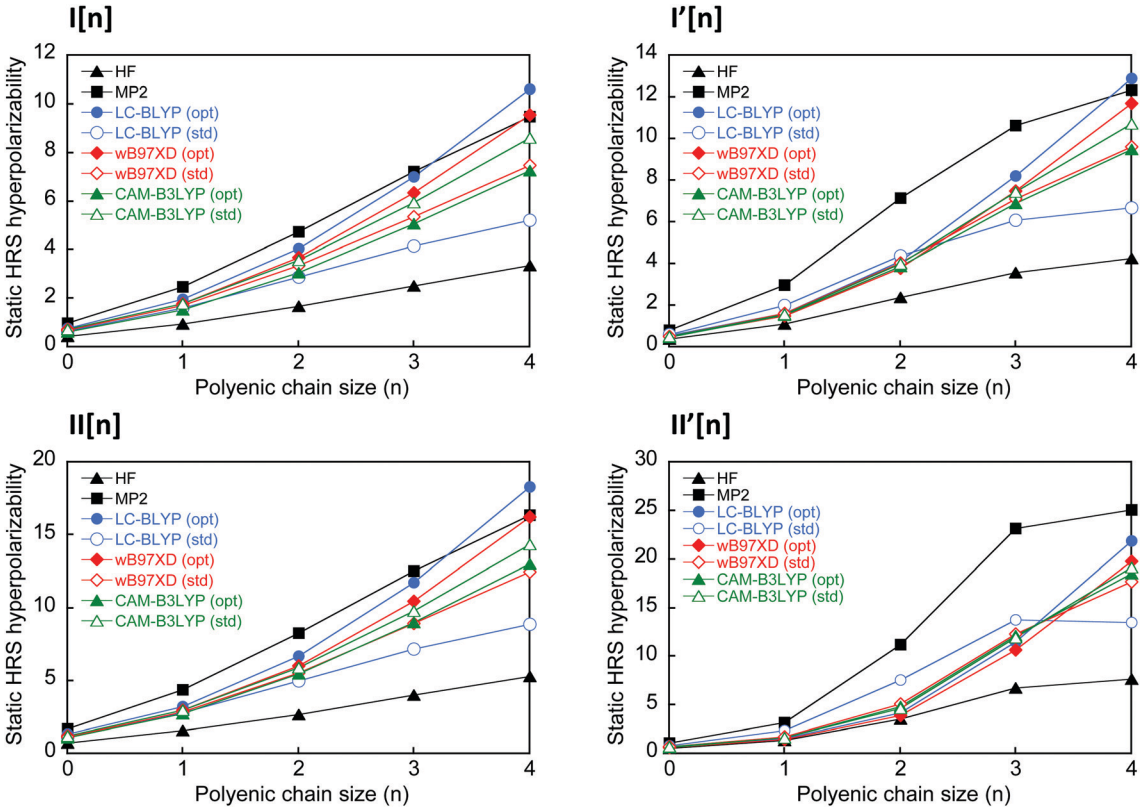

Fig. 8 Evolution of the static HRS hyperpolarizabilities (in 10^4 a.u.) with the length of the polyenic bridge in the four series of merocyanines, calculated in chloroform at the HF, MP2 levels in combination with the 6-311+G(d) basis set, as well as at the DFT level using long-range corrected XC functionals with standard (std) and optimally-tuned (opt) RS parameters.

In series **I′**[*n*] and **II′**[*n*], optimally-tuned LRC XCFs all fail to reproduce the evolution of β_{HRS}^{∞} values as provided by MP2 calculations. Only LC-BLYP with the default ω value reproduces the saturation observed for larger compounds at the CPHF and MP2 levels. Once again, this behavior is linked to the amount of HFX included in the XCF. Optimizing ω lowers the fraction of HFX, so that the saturation of β_{HRS}^{∞} with chain length is expected to appear for chain lengths larger than $n = 4$. It is also interesting to note that ωB97XD using optimally-tuned RS parameters provides β_{HRS}^{∞} values very similar to those calculated at the M06-2X level for the four series of compounds (see Fig. S8, ESI†).

Finally, static hyperpolarizabilities calculated with LC-BLYP using RS parameters optimized in the presence of chloroform are collected in Table S20c (ESI†). Consistently with previous calculations carried out in media of similar optical dielectric constant,[20] the ω values optimized in chloroform (ω_{PCM}) are three times smaller than those optimized in gas phase (Table S3b, ESI†), which drastically reduces the fraction of exact HFX in the functional. Not surprisingly, the resulting β_{HRS}^{∞} values and their evolution with chain length are very similar to that obtained using the BLYP XCF including only DFT exchange (Table S20c, ESI†).

3.3 Frequency dispersion effects

The dynamic HRS hyperpolarizabilities calculated using the Minnesota and long-range corrected functionals, as well as with TDHF are collected in Tables S27–S37 (ESI†) for the four series of compounds. Frequency dispersion factors calculated as $F_{disp} = \beta_{HRS}^{1907}/\beta_{HRS}^{\infty}$, are gathered in Tables S38 and S39 (ESI†), while those estimated from the TSA (F_{disp}^{TSA}, eqn (11)) are collected in Tables S4–S14 (ESI†). Whatever the functional, the two series of values are linearly correlated, which further illustrates the suitability of the TSA to describe this family of compounds. Note that F_{disp} values are systematically smaller than F_{disp}^{TSA}, which originates from the fact that F_{disp} values implicitly include the contribution of higher energy excited states. Note also that the dynamic dielectric constant of chloroform is smaller than the static one, which damps the solvent-induced enhancement of β_{HRS} when going from $\lambda = \infty$ to $\lambda = 1907$ nm, artificially reducing the value of F_{disp}. The same effect is present in F_{disp}^{TSA}, since $\Delta\mu_{01}$ values are calculated using a non-equilibrium solvent approach.

As a result of the lowering of the transition energy, F_{disp} increases with chain length in all families of compounds, with a more pronounced enhancement for the **II** and **II′** series than for **I** and **I′**. In the Minnesota series of functionals, F_{disp} decreases when increasing the amount of HF exchange, as a result of the increase of the transition energy. As for LRC functionals, optimizing the RS parameter induces an exaltation of frequency dispersion effects with LC-BLYP and ωB97X-D, while the ω tuning has no significant effect on F_{disp} values with CAM-B3LYP. For a given compound, frequency dispersion

factors calculated using optimally-tuned ω values evolve in the following order: CAM-B3LYP < ωB97XD < LC-BLYP. Among the Minnesota XCFs, F_{disp} values calculated using M06-2X display the best agreement with those provided by optimally tuned LRC functionals. Thus, M06-2X performs similarly to RS-XCFs not only for evaluating static hyperpolarizabilities as discussed above, but also for gauging the intensification of the NLO responses due to resonance effects. However, none of the

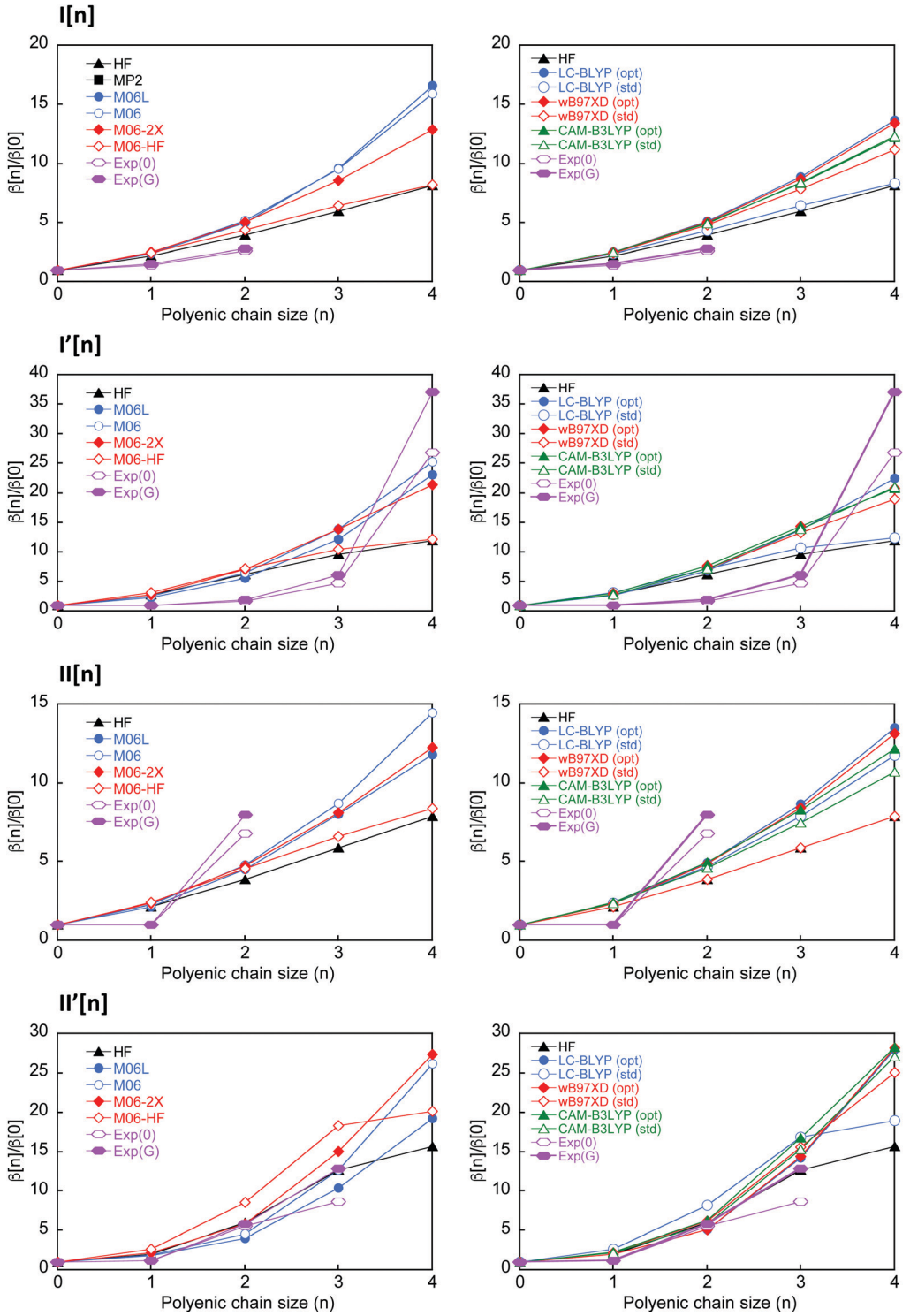

Fig. 9 Evolution of the relative static HRS hyperpolarizabilities ($\beta_{HRS}[n]/\beta_{HRS}[0]$) with the length of the polyenic bridge in the four series of merocyanines, calculated in chloroform using various theoretical levels. Results extrapolated from HRS measurements by using the two-state model either with $\Gamma = 0$ or $\Gamma = 1.2 \times$ HWHM are also reported.

selected XCFs reproduces the experimental frequency dispersion ratios ($F_{disp}(0)$ values in Table 1). Although their global increase with chain length is qualitatively reproduced, frequency resonance effects are largely underestimated for the larger chains, since excitation energies are systematically overestimated. This discrepancy partly originates from the fact that vertical transitions provided by TD-DFT calculations are not strictly comparable to experimental wavelengths of maximal absorption. More physically sound comparisons would require to compute the full vibronic spectra. Furthermore, since the main absorption band of the investigated compounds has a non-symmetrical shape,[23] better estimates of the experimental frequency dispersion factors could also be obtained by considering an intensity-weighted average energy of the transition, instead of the absorption maximum.

3.4 Comparison to experiments

Comparing calculated first hyperpolarizabilities to experimental data measured in or nearby resonant conditions is very tricky. We make here two attempts, both considering relative $\beta_{HRS}[n]/\beta_{HRS}[0]$ rather than absolute β_{HRS} values to enable more reliable comparisons. On the first hand, static β_{HRS} values are compared, where the experimental ones are extrapolated from HRS measurements by using the two-state model (eqn 10), either with $\Gamma = 0$ or $\Gamma = 1.2 \times$ HWHM (see the $\beta^{\infty}_{HRS}(0)$ and $\beta^{\infty}_{HRS}(\Gamma)$ values in Table 1). However, the calculated β^{∞}_{HRS} values cannot be strictly compared to experimental extrapolations, since they are computed using the static dielectric constants ε_0, which differs from the optical dielectric constant that applies for experimental measurements. The solution we adopted to circumvent that issue is to also determine the theoretical static β^{∞}_{HRS} values from the dynamic ones computed at 1907 nm by using the TSA extrapolation procedure (Tables S44 and S45, ESI†).

On the second hand, experimental β^{1907}_{HRS} values are directly compared to the computed dynamic results. Dynamic MP2 values (Tables S40a and b, ESI†) have been obtained by applying a multiplicative approximation in which the static MP2 values are corrected by the F^{TSA}_{disp} ratio calculated at the DFT level using the different XCFs, thus assuming that frequency dispersion and electron correlation effects can be treated independently:[62]

$$\beta^{1907}_{MP2} = \beta^{\infty}_{MP2} \times F^{TSA}_{disp} \quad (14)$$

As illustrated in Fig. 9, the evolution with chain length of theoretical static $\beta^{\infty}_{HRS}[n]/\beta^{\infty}_{HRS}[0]$ ratios correlates at most qualitatively with the experimental data (whether the latter are extrapolated using a damping factor or not). In series **I[*n*]** and **I′[*n*]**, the experimental relative hyperpolarizabilities grows more slowly with n than all computed values for small chain lengths. In **I′[*n*]** they abruptly increase for $n = 4$ as a result of frequency resonance, and get larger than the computed values. The same

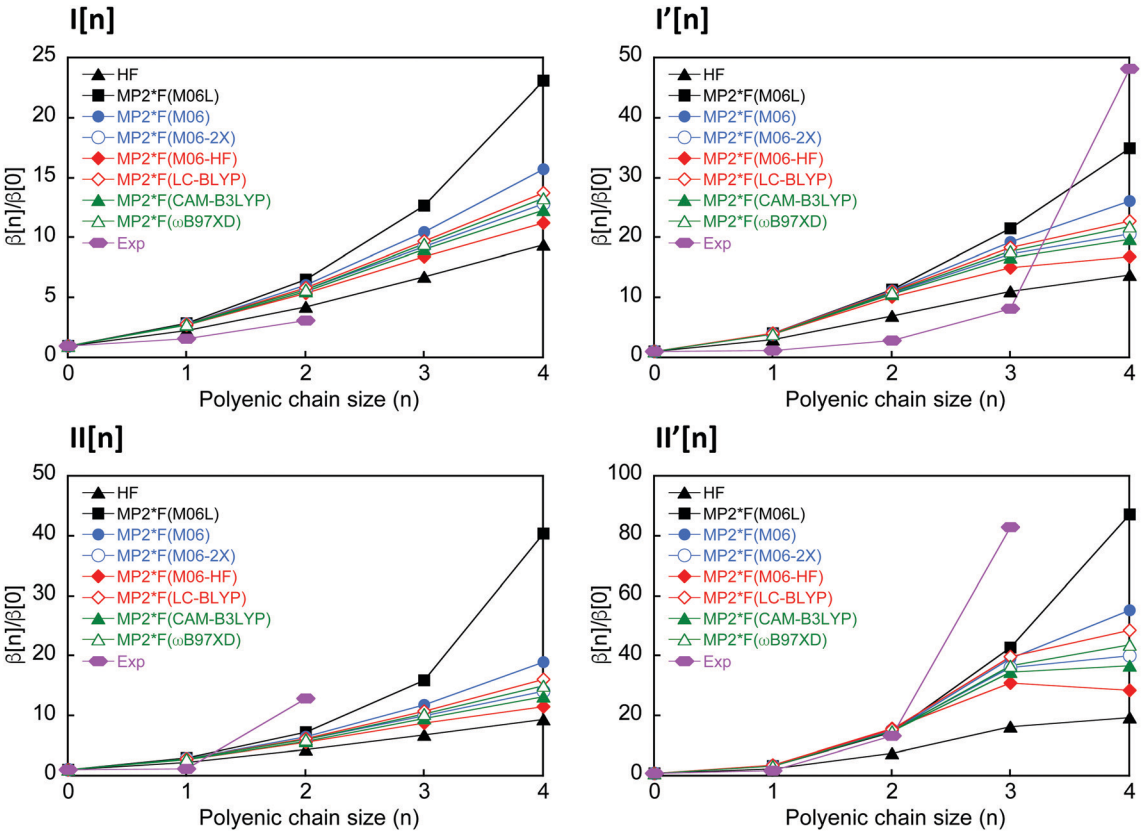

Fig. 10 Evolution of the relative dynamic HRS hyperpolarizabilities ($\beta_{HRS}[n]/\beta_{HRS}[0]$) with the length of the polyenic bridge in the four series of merocyanines, calculated in chloroform at the HF and MP2 levels together with the 6-311+G(d) basis set. MP2 values have been obtained using eqn (14) with frequency dispersion factors calculated using Minnesota and LR-XCFs. Experimental values obtained from HRS measurements are also reported.

behavior is observed from $n = 3$ in the **II[*n*]** series. The agreement between computed and experimental $\beta^{\infty}_{HRS}[n]/\beta^{\infty}_{HRS}[0]$ ratios is better in series **II′[*n*]**. In particular, relative hyperpolarizabilities calculated using hybrid XCFs having a predominant local character (M06L and M06) well reproduce experimental extrapolations issued from the damped TSA. Note that CPHF results are also in good agreement with experiments in this series of compounds.

The evolution with chain length of experimental and theoretical relative β^{1907}_{HRS} values are compared in Fig. S9 and S10 (ESI†). The conclusions do not differ much from the static case. Overall, all calculation levels reproduce qualitatively well the enhancement with chain length of the dynamic first hyperpolarizabilities in the four series of compounds, but fail to reproduce specific results measured in the resonance regime. Whether using the Minnesota (Fig. S9, ESI†) or LR-XCFs (Fig. S10, ESI†), DFT calculations overestimate the $\beta^{1907}_{HRS}[n]/\beta^{1907}_{HRS}[0]$ ratios compared to the experimental ones, except in the resonant cases (**I′[4]**, **II[2]** and **II′[3]**). Dynamic MP2 values obtained using the multiplicative scheme (eqn (14)) show a similar enhancement with n as that obtained at the DFT level (Fig. 10). Note that, except for larger chains ($n = 4$), the choice of the DFT XCF for calculating the frequency dispersion factor F^{TSA}_{disp} has no significant impact.

4 Conclusions

This work investigates the performance of various theoretical levels of approximation to evaluate the second-order NLO responses of recently designed push–pull merocyanine dyes. First hyperpolarizabilities calculated using Minnesota hybrids as well as long-range corrected exchange–correlation functionals are compared to *ab initio* HF and MP2 results, as well as to experimental data obtained from HRS measurements. The evolution of β_{HRS} responses with the nature of the terminal substituents or with the length of the conjugated linker are rationalized by means of the two-state approximation, whose robustness for qualitative interpretations is demonstrated.

The static hyperpolarizabilities calculated using range-separated XCFs globally lie in between values computed at the CPHF and MP2 levels. In most cases, β_{HRS} values computed using LC-BLYP and ωB97XD with optimally-tuned RS parameters are closer to MP2 results than those obtained using default ω values, although the improvement is not systematic and system-dependent. Interestingly, the ω-tuning is shown to attenuate the intrinsic differences in these two XCFs, the β_{HRS} values computed with optimally-tuned RS parameters being closer than those calculated using the default ω values. Contrary to what was found with LC-BLYP and ωB97XD, optimizing the RS parameter in CAM-B3LYP increases the ω values and thus the amount of exact HF exchange in the XCF, which reduces the agreement with MP2 reference results.

Calculations performed using the Minnesota family of functionals evidence that the percentage of exact HF exchange in the XCF strongly impacts the magnitude of the β_{HRS} responses. Interestingly, M06-2X is shown to provide β_{HRS} values in close agreement with optimally tuned range-separated functionals, which indicates that a percentage of nearly 50% between DFT and HF exchange is the adequate balance for computing the NLO properties of these highly dipolar conjugated push–pull chromophores.

This work also illustrates the difficulty to compare the calculated dynamic first hyperpolarizabilities to the experimental data measured in resonance conditions. None of the DFT XCFs considered in this study satisfactorily reproduces the frequency resonance enhancement of the β_{HRS} responses, which hampers any quantitative comparison of their relative evolution with chain length. Using a damped two-state model instead to extrapolate experimental static hyperpolarizabilities does not turn out to be a better strategy to compare theoretical and experimental responses in this series of highly dipolar compounds.

Conflicts of interest

There are no conflicts to declare.

Acknowledgements

This work was supported by the Transnational Common Laboratory QuantumChemPhys: Theoretical Chemistry and Physics at the Quantum Scale (ANR-10-IDEX-03-02), between the Université de Bordeaux (UBx), Euskal Herriko Unibertsitatea (UPV/EHU) and Donostia International Physics Center (DIPC). This research was also funded by Spanish MINECO grant numbers PGC2018-098212-B-C21, EUIN2017-88605 and EUR2019-103825, the Basque Government/Eusko Jaurlaritza (GV/EJ) grant numbers IT1254-19, PIBA19-0004, 2019-CIEN-000092-01 and PRE-2019-2-0168. Calculations were performed on the computing facilities provided by the Mésocentre de Calcul Intensif Aquitain (MCIA) of the University of Bordeaux and of the Université de Pau et des Pays de l'Adour and funded by the Conseil Régional d'Aquitaine, as well as by the Consortium des Equipements de Calcul Intensif (CECI, http://www.ceci-hpc.be), in particular the Technological Platform on High-Performance Computing, financed by the FNRS-FRFC (Conventions No. 2.4.617.07.F and 2.5020.11) and the University of Namur. Unit sphere representations have been generated using the DrawMol software (DrawMol, V. Liégeois, UNamur, www.unamur.be/drawmol).

References

1 L. R. Dalton, P. A. Sullivan and D. H. Bale, Electric Field Poled Organic Electro-optic Materials: State of the Art and Future Prospects, *Chem. Rev.*, 2010, **110**, 25–55.
2 P. J. Campagnola, M. D. Wei and L. M. Loew, High-Resolution Nonlinear Optical Imaging of Live Cells by Second Harmonic Generation, *Biophys. J.*, 1999, **77**, 3341–3349.
3 L. Moreaux, O. Sandre, S. Charpak, M. Blanchard-Desce and J. Mertz, Coherent Scattering in Multi-Harmonic Light Microscopy, *Biophys. J.*, 2001, **80**, 1568–1574.

4 D. A. Dombeck, M. Blanchard-Desce and W. W. Webb, Optical Recording of Action Potentials with Second-Harmonic Generation Microscopy, *J. Neurosci.*, 2004, **24**, 999–1003.
5 J. E. Reeve, H. L. Anderson and K. Clays, Dyes for biological second harmonic generation imaging, *Phys. Chem. Chem. Phys.*, 2010, **12**, 13484–13498.
6 F. Castet, M. Blanchard-Desce, F. Adamietz, Y. M. Poronik, D. T. Gryko and V. Rodriguez, Experimental and Theoretical Investigation of the First-Order Hyperpolarizability of Octupolar Merocyanine Dyes, *ChemPhysChem*, 2014, **15**, 2575–2581.
7 D. R. Kanis, M. A. Ratner and T. J. Marks, Design and construction of molecular assemblies with large second-order optical nonlinearities. Quantum chemical aspects, *Chem. Rev.*, 1994, **94**, 195–242.
8 S. R. Marder, L.-T. Cheng, B. G. Tiemann, A. C. Friedli, M. Blanchard-Desce, J. W. Perry and J. Skindhøj, Large First Hyperpolarizabilities in Push-Pull Polyenes by Tuning of the Bond Length Alternation and Aromaticity, *Science*, 1994, **263**, 511–514.
9 F. Meyers, S. R. Marder, B. M. Pierce and J. L. Brédas, Electric Field Modulated Nonlinear Optical Properties of Donor-Acceptor Polyenes: Sum-Over-States Investigation of the Relationship between Molecular Polarizabilities (.alpha., .beta., and .gamma.) and Bond Length Alternation, *J. Am. Chem. Soc.*, 1994, **116**, 10703–10714.
10 A. Plaquet, B. Champagne, J. Kulhánek, F. Bureš, E. Bogdan, F. Castet, L. Ducasse and V. Rodriguez, Effects of the Nature and Length of the π-Conjugated Bridge on the Second-Order Nonlinear Optical Responses of Push Pull Molecules Including 4,5-Dicyanoimidazole and Their Protonated Forms, *ChemPhysChem*, 2011, **12**, 3245–3252.
11 M. Klikar, P. le Poul, A. Ružička, O. Pytela, A. Barsella, K. D. Dorkenoo, F. Robin-le Guen, F. Bureš and S. Achelle, Dipolar NLO Chromophores Bearing Diazine Rings as π-Conjugated Linkers, *J. Org. Chem.*, 2017, **82**, 9435–9451.
12 *Second-order Nonlinear Optical Characterization Techniques*, ed. T. Verbiest, K. Clays and V. Rodriguez, CRC Press, New York, 2009.
13 K. Pielak, C. Tonnelé, L. Sanguinet, E. Cariati, S. Righetto, L. Muccioli, F. Castet and B. Champagne, Dynamical behavior and second harmonic generation responses in acido-triggered molecular switches, *J. Phys. Chem. C*, 2018, **122**, 26160–26168.
14 M. de Wergifosse and B. Champagne, Electron correlation effects on the first hyperpolarizability of push pull π-conjugated systems, *J. Chem. Phys.*, 2011, **134**, 074113.
15 F. Castet, E. Bogdan, A. Plaquet, L. Ducasse, B. Champagne and V. Rodriguez, Reference molecules for nonlinear optics: A joint experimental and theoretical investigation, *J. Chem. Phys.*, 2012, **136**, 024506.
16 B. Champagne, E. A. Perpéte, D. Jacquemin, S. J. A. van Gisbergen, E.-J. Baerends, C. Soubra-Ghaoui, K. A. Robins and B. Kirtman, Assessment of Conventional Density Functional Schemes for Computing the Dipole Moment and (Hyper)polarizabilities of Push-Pull π-Conjugated Systems, *J. Phys. Chem. A*, 2000, **104**, 4755–4763.
17 L. E. Johnson, L. R. Dalton and B. H. Robinson, Optimizing Calculations of Electronic Excitations and Relative Hyperpolarizabilities of Electrooptic Chromophores, *Acc. Chem. Res.*, 2014, **47**, 3258–3265.
18 F. A. Bulat, A. Toro-Labbé, B. Champagne, B. Kirtman and W. Yang, Density-functional theory (hyper)polarizabilities of push-pull π-conjugated systems: Treatment of exact exchange and role of correlation, *J. Chem. Phys.*, 2005, **123**, 014319.
19 H. Sun and J. Autschbach, Influence of the Delocalization Error and Applicability of Optimal Functional Tuning in Density Functional Calculations of Nonlinear Optical Properties of Organic Donor Acceptor Chromophores, *ChemPhysChem*, 2013, **14**, 2450–2461.
20 A. J. Garza, O. I. Osman, A. M. Asiri and G. E. Scuseria, Can Gap Tuning Schemes of Long-Range Corrected Hybrid Functionals Improve the Description of Hyperpolarizabilities?, *J. Phys. Chem. B*, 2015, **119**, 1202–1212.
21 V. Parthasarathy, R. Pandey, M. Stolte, S. Ghosh, F. Castet, F. Würthner, P. K. Das and M. Blanchard-Desce, Combination of Cyanine Behaviour and Giant Hyperpolarisability in Novel Merocyanine Dyes: Beyond the Bond Length Alternation (BLA) Paradigm, *Chem. – Eur. J.*, 2015, **21**, 14211–14217.
22 V. Parthasarathy, F. Castet, R. Pandey, O. Mongin, P. K. Das and M. Blanchard-Desce, Unprecedented intramolecular cyclization in strongly dipolar extended merocyanine dyes: A route to novel dyes with improved transparency, nonlinear optical properties and thermal stability, *Dyes Pigm.*, 2016, **130**, 70–78.
23 V. Parthasarathy, R. Pandey, P. K. Das, F. Castet and M. Blanchard-Desce, Linear and Nonlinear Optical Properties of Tricyanopropylidene-Based Merocyanine Dyes: Synergistic Experimental and Theoretical Investigations, *ChemPhysChem*, 2018, **19**, 187–197.
24 Y. Zhao and D. G. Truhlar, The M06 Suite of Density Functionals for Main Group Thermochemistry, Thermochemical Kinetics, Noncovalent Interactions, Excited States, and Transition Elements: two New Functionals and Systematic Testing of Four M06-Class Functionals and 12 Other Functionals, *Theor. Chem. Acc.*, 2008, **120**, 215–241.
25 M. Torrent-Sucarrat, S. Navarro, F. P. Cossío, J. M. Anglada and J. M. Luis, Relevance of the DFT method to study expanded porphyrins with different topologies, *J. Comput. Chem.*, 2017, **38**, 2819–2828.
26 I. Casademont-Reig, T. Wöller, J. Contreras-García, M. Alonso, M. Torrent-Sucarrat and E. Matito, New electron delocalization tools to describe the aromaticity in porphyrinoids, *Phys. Chem. Chem. Phys.*, 2018, **20**, 2787–2796.
27 S. J. A. van Gisbergen, J. G. Snijders and E. J. Baerends, Calculating frequency-dependent hyperpolarizabilities using time-dependent density functional theory, *J. Chem. Phys.*, 1998, **109**, 10644–10656.
28 H. Iikura, T. Tsuneda, T. Yanai and K. Hirao, A long-range correction scheme for generalized-gradient-approximation exchange functionals, *J. Chem. Phys.*, 2001, **115**, 3540–3544.

29 T. Yanai, D. P. Tew and N. C. Handy, A new hybrid exchange correlation functional using the Coulomb-attenuating method (CAM-B3LYP), *Chem. Phys. Lett.*, 2004, **393**, 51–57.
30 J.-D. Chai and M. Head-Gordon, Long-range corrected hybrid density functionals with damped atom–atom dispersion corrections, *Phys. Chem. Chem. Phys.*, 2008, **10**, 6615–6620.
31 B. Champagne, P. Beaujean, M. de Wergifosse, M. H. Cardenuto, V. Liégeois and F. Castet, in *Frontiers of Quantum Chemistry*, ed. M. Wojcik, H. Nakatsuji, B. Kirtman and Y. Ozaki, Quantum Chemical Methods for Predicting and Interpreting Second-Order Nonlinear Optical Properties: From Small to Extended π-Conjugated Molecules, Springer, Singapore, 2018, pp. 117–138.
32 B. Mennucci, R. Cammi and J. Tomasi, Medium Effects on the Properties of Chemical Systems: Electric and Magnetic Response of Donor-Acceptor Systems Within the Polarizable Continuum Model, *Int. J. Quantum Chem.*, 1999, **75**, 767–781.
33 J. Tomasi, B. Mennucci and R. Cammi, Quantum Mechanical Continuum Solvation Models, *Chem. Rev.*, 2005, **105**, 2999–3093.
34 M. J. Frisch, G. W. Trucks, H. B. Schlegel, G. E. Scuseria, M. A. Robb, J. R. Cheeseman, G. Scalmani, V. Barone, G. A. Petersson, H. Nakatsuji, X. Li, M. Caricato, A. V. Marenich, J. Bloino, B. G. Janesko, R. Gomperts, B. Mennucci, H. P. Hratchian, J. V. Ortiz, A. F. Izmaylov, J. L. Sonnenberg, D. Williams-Young, F. Ding, F. Lipparini, F. Egidi, J. Goings, B. Peng, A. Petrone, T. Henderson, D. Ranasinghe, V. G. Zakrzewski, J. Gao, N. Rega, G. Zheng, W. Liang, M. Hada, M. Ehara, K. Toyota, R. Fukuda, J. Hasegawa, M. Ishida, T. Nakajima, Y. Honda, O. Kitao, H. Nakai, T. Vreven, K. Throssell, J. A. Montgomery Jr., J. E. Peralta, F. Ogliaro, M. J. Bearpark, J. J. Heyd, E. N. Brothers, K. N. Kudin, V. N. Staroverov, T. A. Keith, R. Kobayashi, J. Normand, K. Raghavachari, A. P. Rendell, J. C. Burant, S. S. Iyengar, J. Tomasi, M. Cossi, J. M. Millam, M. Klene, C. Adamo, R. Cammi, J. W. Ochterski, R. L. Martin, K. Morokuma, O. Farkas, J. B. Foresman and D. J. Fox, *Gaussian 16 Revision C.01*, Gaussian Inc., Wallingford CT, 2016.
35 T. Stein, L. Kronik and R. Baer, Prediction of charge-transfer excitations in coumarin-based dyes using a range-separated functional tuned from first principles, *J. Chem. Phys.*, 2009, **131**, 244119.
36 T. Stein, L. Kronik and R. Baer, Reliable Prediction of Charge Transfer Excitations in Molecular Complexes Using Time-Dependent Density Functional Theory, *J. Am. Chem. Soc.*, 2009, **131**, 2818–2820.
37 T. Stein, H. Eisenberg, L. Kronik and R. Baer, Fundamental Gaps in Finite Systems from Eigenvalues of a Generalized Kohn-Sham Method, *Phys. Rev. Lett.*, 2010, **105**, 266802.
38 A. Karolewski, T. Stein, R. Baer and S. Kümmel, Communication: Tailoring the optical gap in light-harvesting molecules, *J. Chem. Phys.*, 2011, **134**, 151101.
39 J. Kiefer, Sequential minimax search for a maximum, *Proc. Am. Math. Soc.*, 1953, **4**, 502–506.
40 T. Körzdörfer, J. S. Sears, C. Sutton and J.-L. Brédas, Long-range corrected hybrid functionals for π-conjugated systems: Dependence of the range-separation parameter on conjugation length, *J. Chem. Phys.*, 2011, **135**, 204107.
41 L. Pandey, C. Doiron, J. S. Sears and J.-L. Brédas, Lowest excited states and optical absorption spectra of donor acceptor copolymers for organic photovoltaics: a new picture emerging from tuned long-range corrected density functionals, *Phys. Chem. Chem. Phys.*, 2012, **14**, 14243–14248.
42 K. Garrett, X. Sosa Vazquez, S. B. Egri, J. Wilmer, L. E. Johnson, B. H. Robinson and C. M. Isborn, Optimum Exchange for Calculation of Excitation Energies and Hyperpolarizabilities of Organic Electro-optic Chromophores, *J. Chem. Theory Comput.*, 2014, **10**, 3821–3831.
43 P. Besalú-Sala, S. P. Sitkiewicz, P. Salvador, E. Matito and J. M. Luis, A new tuned range-separated density functional for the accurate calculation of second hyperpolarizabilities, *Phys. Chem. Chem. Phys.*, 2020, **22**, 11871–11880.
44 R. Zaleśny, M. Medved', S. P. Sitkiewicz, E. Matito and J. M. Luis, Can Density Functional Theory Be Trusted for High-Order Electric Properties? The Case of Hydrogen-Bonded Complexes, *J. Chem. Theory Comput.*, 2019, **15**, 3570–3579.
45 H. Reis, Problems in the comparison of theoretical and experimental hyperpolarizabilities revisited, *J. Chem. Phys.*, 2006, **125**, 014506.
46 J. L. Oudar and D. S. Chemla, Hyperpolarizabilities of the Nitroanilines and Their Relations to the Excited State Dipole Moment, *J. Chem. Phys.*, 1977, **66**, 2664–2668.
47 T. Le Bahers, C. Adamo and I. Ciofini, A Qualitative Index of Spatial Extent in Charge-Transfer Excitations, *J. Chem. Theory Comput.*, 2011, **7**, 2498–2506.
48 D. Jacquemin, T. L. Bahers, C. Adamo and I. Ciofini, What is the ''best'' atomic charge model to describe through-space charge-transfer excitations?, *Phys. Chem. Chem. Phys.*, 2012, **14**, 5383–5388.
49 J. Campo, F. Desmet, W. Wenseleers and E. Goovaerts, Highly sensitive setup for tunable wavelength hyper-Rayleigh scattering with parallel detection and calibration data for various solvents, *Opt. Express*, 2009, **17**, 4587–4604.
50 As reported in ref. 49, λ_{max} = 481 nm and $\beta^{\infty}_{zzz} = 160 \times 10^{-30}$ esu = 18516 a.u. for DR1 in chloroform. Assuming that DR1 has a quasi $C_{\infty v}$ symmetry, $\beta^{\infty}_{HRS} = \sqrt{\frac{6}{35}} \times \beta^{\infty}_{zzz} = 7667$ a.u. At 1907 nm, $F^{TSA}_{disp} = 1.43$, so that $\beta^{1907}_{HRS} = \beta^{\infty}_{HRS} \times F^{TSA}_{disp} = 7667 \times 1.43 = 10\,963$ a.u.
51 G. Berkovic, G. Meshulam and Z. Kotler, Measurement and analysis of molecular hyperpolarizability in the two-photon resonance regime, *J. Chem. Phys.*, 2000, **112**, 3997–4003.
52 F. Mançois, J.-L. Pozzo, J. Pan, F. Adamietz, V. Rodriguez, L. Ducasse, F. Castet, A. Plaquet and B. Champagne, Two-Way Molecular Switches with Large Nonlinear Optical Contrast, *Chem. – Eur. J.*, 2009, **15**, 2560–2571.
53 P. Beaujean, F. Bondu, A. Plaquet, J. Garcia-Amorós, J. Cusido, F. M. Raymo, F. Castet, V. Rodriguez and B. Champagne,

Oxazines: A New Class of Second-Order Nonlinear Optical Switches, *J. Am. Chem. Soc.*, 2016, **138**, 5052–5062.

54 F. Castet, A. Pic and B. Champagne, Linear and nonlinear optical properties of arylvinyldiazine dyes: A theoretical investigation, *Dyes Pigm.*, 2014, **110**, 256–260.

55 A. Tuer, S. Krouglov, R. Cisek, D. Tokarz and V. Barzda, Three-dimensional visualization of the first hyperpolarizability tensor, *J. Comput. Chem.*, 2011, **32**, 1128–1134.

56 Arrows represent the effective second-order induced dipoles $\vec{\mu}_{\text{eff}} = \overrightarrow{\overleftrightarrow{\beta}} : \vec{F}^2(\theta, \phi)$ plotted at each point (θ,ϕ) of the surface of a sphere centered at the center of mass of the molecules, where $\overrightarrow{\overleftrightarrow{\beta}}$ is the first hyperpolarizability tensor and $\vec{F}$ a unit vector of the incident electric field with polarization defined in the spherical coordinates (θ,ϕ).

57 J. C. Sancho-García and A. J. Pérez-Jiménez, Improved accuracy with medium cost computational methods for the evaluation of bond length alternation of increasingly long oligoacetylenes, *Phys. Chem. Chem. Phys.*, 2007, **9**, 5874–5879.

58 G. Bourhill, J.-L. Bredas, L.-T. Cheng, S. R. Marder, F. Meyers, J. W. Perry and B. G. Tiemann, Experimental Demonstration of the Dependence of the First Hyperpolarizability of Donor-Acceptor-Substituted Polyenes on the Ground-State Polarization and Bond Length Alternation, *J. Am. Chem. Soc.*, 1994, **116**, 2619–2620.

59 C. B. Gorman and S. R. Marder, Effect of Molecular Polarization on Bond-Length Alternation, Linear Polarizability, First and Second Hyperpolarizability in Donor-Acceptor Polyenes as a Function of Chain Length, *Chem. Mater.*, 1995, **7**, 215–220.

60 M. Barzoukas, A. Fort and M. Blanchard-Desce, Quadratic hyperpolarizability of push - pull polyenes: a two-form analysis of the length effect, *Synth. Met.*, 1996, **83**, 277–280.

61 S. Nénon, B. Champagne and M. I. Spassova, Assessing long-range corrected functionals with physically-adjusted range-separated parameters for calculating the polarizability and the second hyperpolarizability of polydiacetylene and polybutatriene chains, *Phys. Chem. Chem. Phys.*, 2014, **16**, 7083–7088.

62 H. Sekino and R. J. Bartlett, Hyperpolarizabilities of molecules with frequency dependence and electron correlation, *J. Chem. Phys.*, 1991, **94**, 3665–3669.

